

Sound Convergence Zones Formed by Reflection from the Sea Bottom in an Incomplete Sound Channel*

Peng Zhang^{1,2}, Zhenglin Li¹, Lixin Wu¹, Renhe Zhang¹, Jixing Qin¹

¹State Key Laboratory of Acoustics, Institute of Acoustics, Chinese Academy of Sciences, Beijing 100190, China.

²College of Electronic Electrical and Communication Engineering, University of Chinese Academy of Sciences, Beijing 100049, China.
lzhl@mail.ioa.ac.cn

ABSTRACT

The seafloor has a significant influence on sound propagation in deep water in the context of an incomplete sound channel. Using data collected during an experiment in the South China Sea, we study seafloor reflection effects on sound propagation in a range dependent environment. The experiment phenomenon is different from the convergence phenomenon in the deep sound channel, also referred to as the SOFAR channel. We observe that the spatial variation of bathymetry contributes to the formation of the seafloor reflection convergence zone in advance, and the sound intensity in some areas of the shadow zone is significantly increased. Due to seafloor reflection, there are two seafloor reflection convergence zone within 60 km of the propagation track, in which the gains of the acoustic energy can exceed 10 dB. High sound intensity areas are also observed in the shadow zone near 11 km and 51 km at some depths. In addition, the gain of the second convergence zone is higher than that of the first convergence zone when the receiving depth is the same as the source depth. In the first convergence zone, as the receiving depth increases, the arrival structure tends to become complicated, and the multipath effect becomes more obvious. Numerical analysis based on the parabolic equation and ray theory is carried out to explain the physical mechanism of the seafloor reflection convergence zone. The study result is meaningful for the performance analysis of sonar in complex deep-water environments.*

KEYWORDS

convergence zone, bottom reflection, multipath structure

ACM Reference format:

Peng Zhang, Zhenglin Li, Lixin Wu, Renhe Zhang, and Jixing Qin. 2018. Sound Convergence Zones Formed by Reflection from the Sea Bottom in an Incomplete Sound Channel. In *The 13th ACM International Conference on Underwater Networks & Systems (WUWNet'18), December 3–5, 2018, Shen zhen, China*, (Eds.). ACM, New York, NY, USA, Article , 5 pages.
<https://doi.org/10.1145/3291940.3291985>

Permission to make digital or hard copies of all or part of this work for personal or classroom use is granted without fee provided that copies are not made or distributed for profit or commercial advantage and that copies bear this notice and the full citation on the first page. Copyrights for components of this work owned by others than ACM must be honored. Abstracting with credit is permitted. To copy otherwise, or republish, to post on servers or to redistribute to lists, requires prior specific permission and/or a fee. Request permissions from Permissions@acm.org.
WUWNet'18, December 3–5, 2018, Shenzhen, China

© 2018 Association for Computing Machinery.

ACM ISBN 978-1-4503-6193-4/18/12...\$15.00

<https://doi.org/10.1145/3291940.3291985>

1 INTRODUCTION

Convergence zones of the sound field are formed by variations of the sound speed profile and water depth, which is an important acoustic characteristic in deep water. Prior to the twenty-first century, a series of sound propagation experiments were conducted to elucidate the issues of convergence effect. Hale [1] observed a strong convergence zone effect in a deep water experiment in the early 1960s. Ray theory [2], wave theory [3,4] and extended theories [5] were applied to study the convergence zone over the next few decades. These theories profoundly revealed the mechanisms of sound propagation and could accurately predict the location of the convergence zone. Discussions in these research papers focused on sound propagation in typical SOFAR channels. In the far field of the SOFAR channel, the influence of the sea floor can be ignored because most rays are reflected by sea water before touching the seafloor. But in an incomplete channel, the sound field is mainly formed by sound waves reflected from the seabed. The characteristics of seabed sediment therefore become important factors affecting sound propagation.

Applying the theory of reversal point convergence zone, Zhang Renhe [6] calculated the seafloor reflection coefficient of the minimum glancing angle under the negative gradient profile environment. However, the acoustic characteristics of the seabed were not directly described in this paper. In addition, the theoretical calculation does not match the experimental results with regard to the location and gain of the convergence zone. Wang Gang et al. [7] applied the WKBZ normal wave method to study the seafloor reflection convergence zone under the deep sea negative gradient depth profile. Fan Peiqin et al. [8] simulated rapid distance prediction of the seafloor reflection convergence zone by using environment statistical data and the characteristic parameter calculation model. Many researchers have looked at the effects of acoustic propagation in range-dependent underwater environments, such as the reflection blocking effect of the seamount [9], acoustic propagation lows along uneven bottoms [10], and down-slope enhancement effects [11].

In this paper, sound propagation experiment data collected in the South China Sea is used to analyze the characteristics of the convergence zone formed by bottom reflection under the incomplete channel environment with variation of bathymetry. Numerical analysis based on the parabolic equation combined with ray theory is carried out to calculate the arrival time of the pulse arrival structure as well as the eigenrays and explain the

physical causes of the seafloor reflection convergence phenomenon.

2 SOUND PROPAGATION IN THE INCOMPLETE CHANNEL

2.1 Description of the Experiment

In April 2018, a comprehensive experiment was carried out by the State Key Laboratory of Acoustics, Chinese Academy of Sciences in the South China Sea. One of the main purposes was to study sound propagation characteristics in the complex deep water environment. The sound source was towed by the experiment's ship away from a receiving vertical line array (VLA). The VLA consisted of 20 hydrophones placed from 85 m to 3400 m with an unequal depth space. The sensitivities of the hydrophones were -170 dB, and the sampling rate of the signal was 16 kHz. The acoustic source was towed at a speed of 4 knots, transmitting a hyperbolic frequency modulated (HFM) signal with a frequency range from 250 Hz to 350 Hz. The depth of the towed transducer was about 150 m, and the emission source level was 192 dB.

The bathymetry along the propagation track is shown in Fig. 1. We can see there is a small seamount with a height of 500 m within 20 km of the propagation track and the topography is undulating. The sea bottom in the range from 20 km to 60 km is relatively flat.

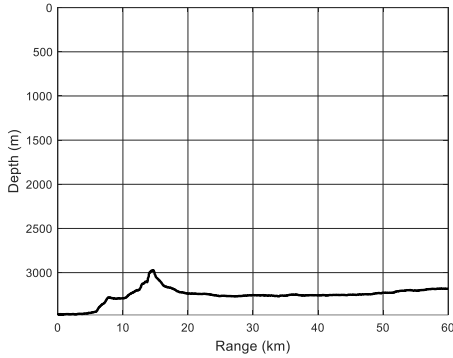


Fig. 1 The bathymetry along the propagation track.

During the experiment, the sound speed profile of seawater was measured every 10 km using a conductivity temperature depth (CTD) and expendable bathythermograph (XBT). The sound speed profile change at different distances is small, and the sound speed profile at the receiving position is shown in Fig. 2. The maximum measured depth of the sound speed profile is 1200 m, so the sound speed profile below 1200 m is taken from the data base. We see that it is a typical incomplete deep water sound channel. The channel axis is located near the depth of 1100 m. The sound speed at the deepest part of the seabed is 1515 m/s, which is less than the sound speed of 1539 m/s near the sea surface. The black dots indicate the depth of the 20 VLA hydrophones, the blue dotted line indicates the depth of the towed sound source, and the solid blue line indicates the sound

speed at the depth of the deep source, which is close to the speed of sound near the bottom. For the range larger than 10 km, the sound speed near the seabed is much smaller than that of the source depth. Thus, the sound reflection from the sea bottom cannot be ignored.

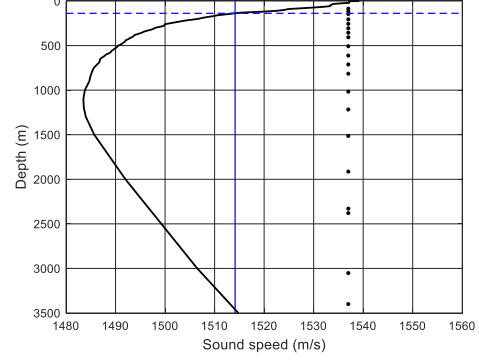


Fig. 2 Sound speed profile during the experiment.

2.2 Experimental Results

Assume that $x_n(t)$ denotes the signal received by one of the hydrophones on the VLA.

$$x_n(t) = \int X(\omega)H(r, z; \omega)\exp(-i\omega t)d\omega \quad (1)$$

where $X(\omega)$ is the spectrum of original acoustic emission signals and $H(r, z; \omega)$ is the transfer function of sound channel from source to receiver. The pulse compression method is used to improve the signal-to-noise ratio (SNR)

$$x_c(t) = \int |X(\omega)|^2 H(r, z; \omega)\exp(-i\omega t)d\omega \quad (2)$$

The fast Fourier transform (FFT) operation is then applied to obtain the spectrum X_i of at i -th frequency bin. The measured spectra are averaged in the frequency bandwidth (100 Hz) of the signal, and the average energy of the signal is expressed as

$$E(f_0) = \frac{2}{F_s^2} \frac{1}{nf_2 - nf_1 + 1} \sum_{i=nf_1}^{nf_2} |X_i|^2 \quad (3)$$

where f_0 is the central frequency, F_s is the sampling rate, nf_1 and nf_2 are the numbers at the start and end frequency for the frequency band, respectively. Then the transmission loss (TL) can be denoted as

$$TL(f_0) = SL(f_0) - (10\lg[E(f_0)] - M_v - E_c) \quad (4)$$

where $SL(f_0)$ is the source level of the transducer, M_v is the sensitivity of the hydrophones, and E_c represents the increasing energy of the pulse compression filter.

Finally, the two-dimensional TL along the experiment track is shown in Fig. 3. It is clear that two distinct convergence zones

can be observed over a distance of 60 km, which are located near 20 km and 40 km, respectively. At the same time, two more obvious acoustic enhancement areas can be observed around 11 km and 51 km.

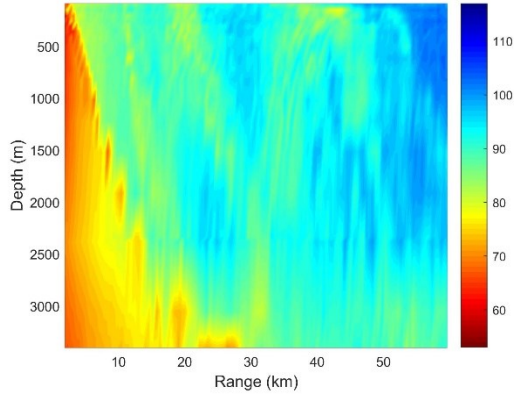


Fig. 3 Two dimensional experimental TLs

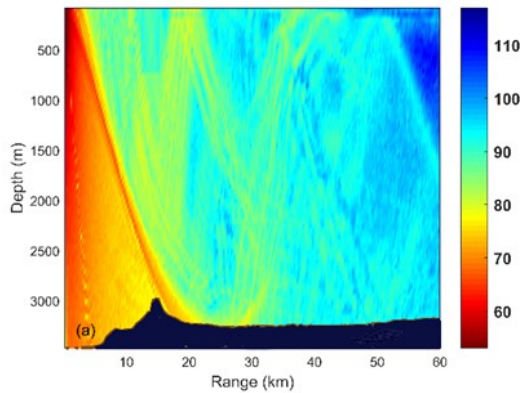


Fig. 4 Numerical TLs results from RAM-PE model.

The parabolic equation method (RAM-PE [10,11]) is used to calculate TLs to analyze the experimental phenomena. Selections of the central frequency and bandwidth of the sound source are the same as the experiment ones, with the frequency interval of 10 Hz and the frequency point number of 11. A two-layer fluid bottom model is selected with a sediment thickness of 20 m, sediment sound speed of 1499 m/s, and sediment density of 1.36 g/cm³ (according to the sampling results), and the infinite basement has a sound speed of 1650 m/s and density of 1.8 g/cm³. The attenuation coefficients are chosen as $0.517 \times (f/1000)^{1.07}$ dB/ λ [12]. Because the hydrophone placed under the channel axis is sparse in the experiment, the TL in Fig. 3 is not smooth due to the interpolation. So the receiving depth below the channel axis is increased in PE calculation, and the numerical TLs results are shown in Fig. 4.

Comparing Fig. 3 with Fig. 4, we can see that the numerical results are consistent with the experimental TL. There are two

obvious convergence zones within 60 km of the real bathymetry. Some rays are reflected from the seamount and converge at 20 km, which is the reason for the formation of the first convergence zone. Some of the direct-arrival rays and rays from the first convergence zone are reflected from the sea bottom, and then they arrive near the sea surface at around 40 km, which leads to the formation of the second reflection convergence zone.

To quantitatively analyze the experimental phenomena, Fig. 5 shows the TLs comparisons at two typical receiving depths (85 m and 145 m). We can further confirm that two convergence zones appear near 20 km and 40 km. The gains of the two convergence zones can be achieved at more than 10 dB, and the sound intensity of the second convergence zone at the depth of 145 m and 42 km distance is higher than that at the first convergence zone at the same receiving depth. In addition, there are also two areas with high sound intensity near 11 km and 51 km at the depth of 145 m, where the gain is less than those of the two convergence zones. However, there is only one acoustic enhancement zone at 11 km and 85 m receiving depth, and the sound intensity enhancement zone cannot be observed at 51 km. The calculated results are consistent with the experimental results.

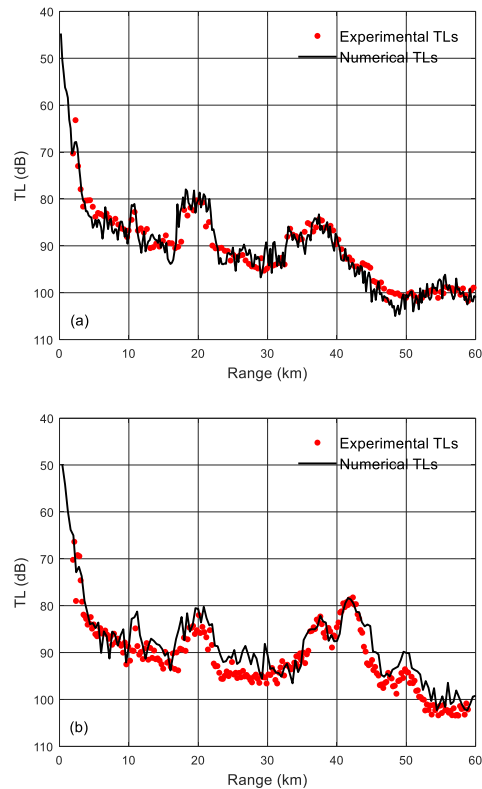


Fig. 5 Comparison of experimental TLs and numerical TLs, where(a)-(b) for the receivers at 85 m and 145 m, respectively.

3 THEORETICAL EXPLANATION

To explain the seafloor reflection convergence phenomenon observed during the experiment, ray theory is used for analysis. Following the principle of reciprocity, Fig. 6 shows the sound rays' traces at two different receivers. The black dot at 0 km indicates the source depth, and the black dotted line indicates a receiver depth of 150m. In Fig. 6, the rays reflected by the sea surface and seabed reflection (many times) are depicted by the blue-green line, the rays reflected by the sea bottom (only once) are depicted by the red line, and the blue line indicates a sound

line that is only refracted by sea water and is not reflected by either bottom or surface.

The sound speed near the sea bottom is close to that near the source depth. Except for a few small glancing angles, most other sound ray traces cannot be refracted before reaching the sea bottom and will be reflected by the seafloor, which is consistent with the simulation results in Fig. 6. We can see a large number of sound rays arriving near 11 km, 20 km, and 40 km at the two receiving depths, corresponding to the high intensity area and the two seafloor reflection convergence zones in Fig. 5. We find that the grazing angles of the sound rays reaching the second

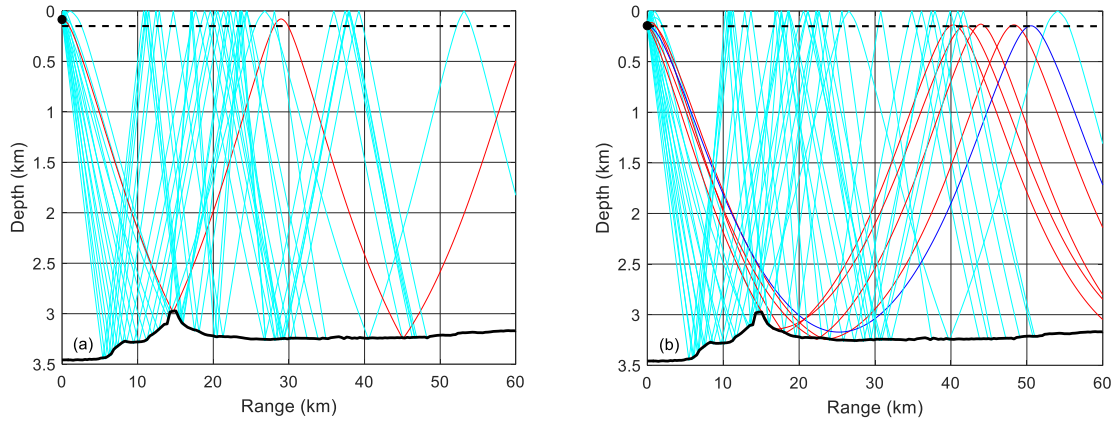


Fig. 6 Ray traces at two different receivers, (a) for 85m and (b) for 150m. Black dots mark the source depth, and the black dashed line indicates the receiver depth at 150m.

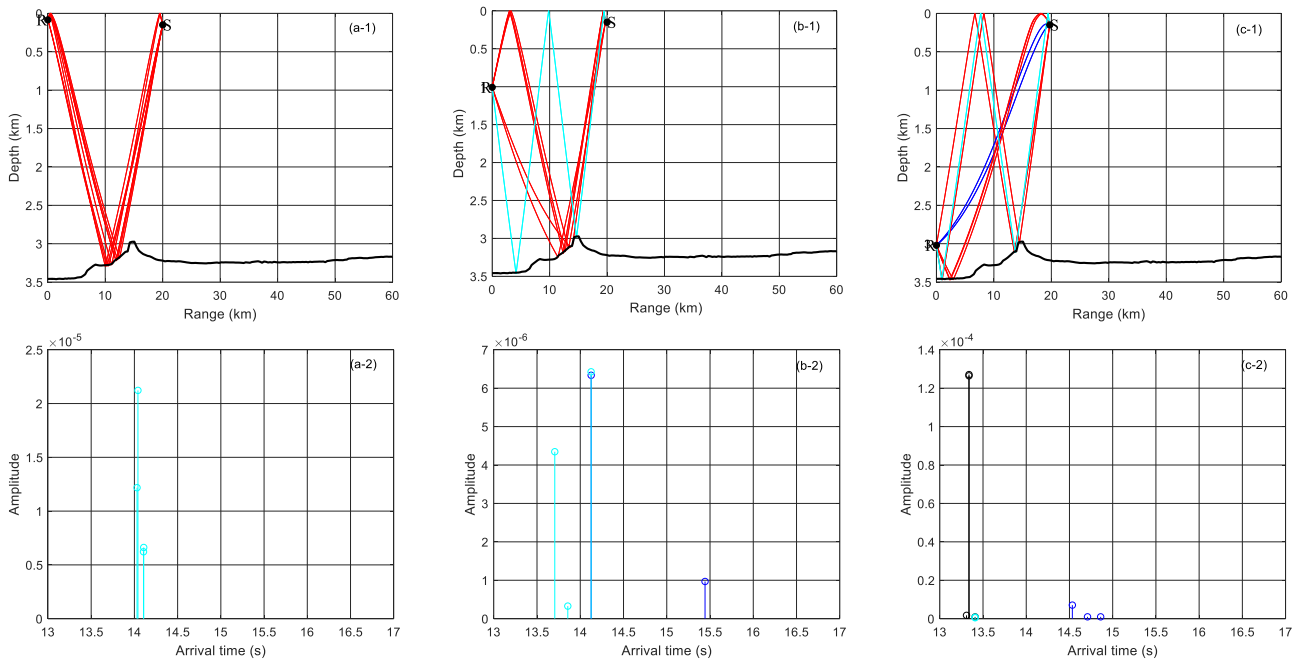


Fig. 7 Comparison of eigenrays and arrival structures at different receiver depths in the first bottom reflection convergence zone: (a) for the receiver depth at 85 m, (b) for the receiver depth at 1008 m, and (c) for the receiver depth of 3021 m.

convergence zone are smaller than those of the first convergence zone, and the seafloor reflection loss for the rays with smaller glancing angles is smaller, which causes a higher gain in the second convergence zone. Some rays arrive at the range of 51 km for the receiver depth of 145m, which is refracted by the water and forms a relatively high acoustic intensity region. But those refracted rays cannot arrive at the receiver depth of 85 m because the sound speed at 85 m is much greater than that near the bottom.

Comparing the ray traces for two different depths in Fig. 6, the existence of the seamount contributes to the formation of the seafloor reflection convergence zone in advance. Fig. 7 shows the eigenrays and arrival structure at different receiver depths (85 m, 1008 m, and 3021 m) in the first reflection convergence zone (20 km). We find that the range of the seafloor reflection area becomes larger as the receiver depth increases, and arrival structures tend to become more complicated.

4 CONCLUSIONS

In April 2018, a propagation experiment was conducted in the South China Sea, with a towed sound source and VLA. The observed phenomenon is quite different from the convergence phenomenon in the typical deep water environment. Numerical analysis based on the parabolic equations combined with ray theory was carried out to explain the formation mechanism of the seafloor reflection convergence zone in deep water with a complex seafloor environment. The experimental and numerical results show that changes in seabed topography greatly influence the formation and propagation characteristics of the seafloor reflection convergence zone within the range of the direct-arrival sound area. As the sea depth becomes gradually shallower with increasing distance, the convergence zone under the SOFAR channel is destroyed. Two obvious seafloor reflection convergence structures are observed at distances of 20 km and 40 km, in which the gain is up to 10 dB. Some high sound intensity areas are formed in the shadow zone due to the reflection of the sea floor or the refraction of seawater. When the source and receiver are located at the same depth, the gain of the second convergence zone is higher than that of the first convergence zone, which is caused by the decrease in the bottom reflection energy loss and the increase in the number of arriving rays. In the first reflection convergence zone, as the receiver depth increases, the multipath effect is more obvious. The results are meaningful for SONAR performance analysis.

ACKNOWLEDGMENTS

The authors thank all the staff for participating in the experiment conducted in South China Sea in 2018.

This project is supported by the National Natural Science Foundation of China (Grant Nos. 11434012, 41561144006, 11874061).

REFERENCES

[1] Hale F E. 1961. Long-Range Sound Propagation in the Deep Ocean. *J. Acoust. Soc. Am* 33(4), 456-464
 [2] Urlick R J. 1965. Caustics and Convergence Zones in Deep-Water Sound Transmission. *J. Acoust. Soc. Am* 38(2), 348-358.

[3] Brekhovskikh L M, Lysanov Yu P. 2003. Fundamentals of Ocean Acoustics (3rd. ed.). Springer, New York, NY.
 [4] Williams A O, Horul W. 1967. Axial focusing of sound in the SOFAR channel. *J. Acoust. Soc. Am* 41(1), 189-198.
 [5] Zhang RH. 1980. Turing-point convergence zones in underwater sound channel(I) A normal-mode theory. *Acta Acust* 1 30-42.
 [6] Zhang RH, Sun GC, Lei LY, Zhou JL. 1985. Turing-point convergence zones in the deep sea with negative velocity gradient. *Acta Acust* 2, 93-96.
 [7] Wang G. 1995. On the study of turning-point convergence-zones formed by sound reflection from the sea bottom in deep ocean. Master's thesis. Institute of Acoustics, Chinese Academy of Sciences, Beijing, China.
 [8] Fan PQ, Da LL, Li YY. 2013. The research of reflected convergence zones range computing method in deep ocean. *Tech. Acoust* 32(6), 71-72
 [9] Li W, Li ZL, Zhang RH. 2015. The effects of seamounts on sound propagation in deep water. *Chin Phys Lett* 32(6), 103-106.
 [10] Hu ZG, Li ZL, Zhang RH, Ren Y, Qin JX, He L. 2016 Sound propagation in deep water with a sloping bottom. *Acta Phys. Sin.* 65(1), 221-229
 [11] Qin JX, Zhang RH, Luo WY, Wu LX, Jiang L, Zhang B. 2014. Two-dimensional sound propagation over a continental slope. *Acta Acust* 39(2) 145-153.
 [12] Li Z, Li F. 2010. Geoacoustic inversion for sediments in the South China Sea based on a hybrid inversion scheme. *Chin J Ocean Limnol.* 28(5),990-995.
 [13] Jensen F, Kuperman W, Porter M, and Schmidt H. 2011 Computational Ocean Acoustics (2nd. ed.). Springer, Berlin.